**Proceedings of the 2025 SICE Festival with Annual Conference**
**September 9-12, 2025, Chiang Mai, Thailand**

# A Simple Head-Trunk-Limb Coordination Control Capable of Three Types of Quadruped Galloping

Goku Sawada[1†] Seokhyun Kim[1] Shura Suzuki[1]
Kotaro Yasui[1] Akira Fukuhara[1] Akio Ishiguro[1]

[1]Tohoku University, Sendai, Japan
(E-mail: sawada.goku.r7@dc.tohoku.ac.jp, shura.suzuki.c6@tohoku.ac.jp)

**Abstract:** Gallop is the fastest gait employed by quadruped animals, with variations in flight timing which characterize periods when all limbs are off the ground. While previous studies have investigated gallop dynamics with various flight timings using analytical or optimization approaches, the underlying control mechanisms that determine these flight timings remain insufficiently explored. In this study, we investigate the control mechanisms underlying galloping gaits through mathematical modeling and simulations. Our results showed that the strength of the head and trunk actuation serves as a determinant for flight timing variations in gallop gait.

**Keywords:** Quadruped robot, Whole-body coordination, Galloping

## 1. INTRODUCTION

Quadruped animals achieve remarkable locomotion speeds in complex natural environments. Cheetahs can reach speeds exceeding 100 km/h, while horses can maintain speeds of 30 km/h over an hour [1], far surpassing the mobility capabilities of state-of-the-art legged robots [2]. Understanding the underlying mechanisms that enable such high mobility in quadruped animals helps design agile quadruped robots, as well as contributes to biological knowledge.

Gallop is the fastest gait employed by quadruped animals, with variations in footfall sequence and flight timing [3]. Footfall sequence distinguishes between transverse gallop (left-hind, right-hind, left-fore, right-fore) and rotary gallop (left-hind, right-hind, right-fore, left-fore). Flight timing, which characterizes periods when all limbs are simultaneously off the ground, categorizes galloping into four types: gathered flight (after fore limbs leave), extended flight (after hind limbs leave), dual flight (after both limbs leave), and no flight (where at least one limb always maintains ground contact). These galloping patterns vary across species and can shift with changes in locomotion speed [3]. Therefore, understanding the mechanism of galloping, which involves multiple patterns, is key for revealing high-speed locomotion in quadrupeds.

Simulation and robotic approaches have been conducted to investigate the underlying mechanisms of galloping. For example, Kamimura et al. explored the mechanical basis for differences between rotary and transverse gallops, and examined the factors contributing to cheetahs' use of dual flight patterns [4, 5]. Alqham et al. compared the speed and energy efficiency of 16 galloping types characterized by different gait and flight patterns [6]. Although these works provided valuable insights into galloping dynamics, the motor control mechanisms that determine galloping flight timing have not been sufficiently explored.

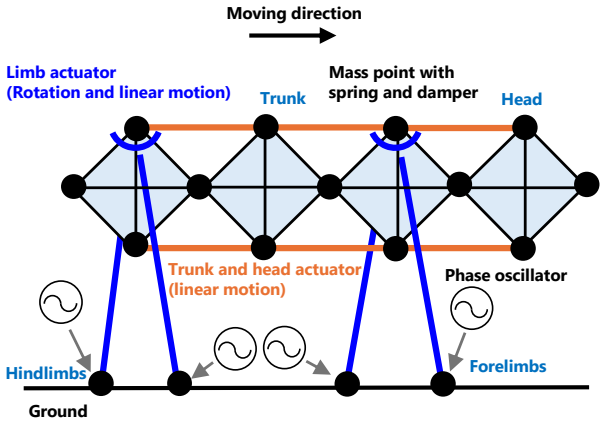


Fig. 1: Schematic of quadruped model.

From the motor control perspective, previous studies modeled an intraspinal neural network of quadruped animals such as central pattern generator (CPG) that produce basic locomotion rhythm and patterns [7]. Owaki and Ishiguro, as well as Fukuhara et al., proposed control methods that generate a transverse gallop using foot force sensory feedback [8, 9]. Furthermore, Suzuki et al. proposed a control strategy that utilizes foot force and neck movement information to produce a rotary gallop [10]. In addition, Fukuoka et al. and Fukui et al. demonstrated that both transverse and rotary gallops can be generated by utilizing body tilt angle information [11, 12].

This study aims to investigate the factors of gallop variation from the aspect of motor control. We

† Goku Sawada is the presenter of this paper.

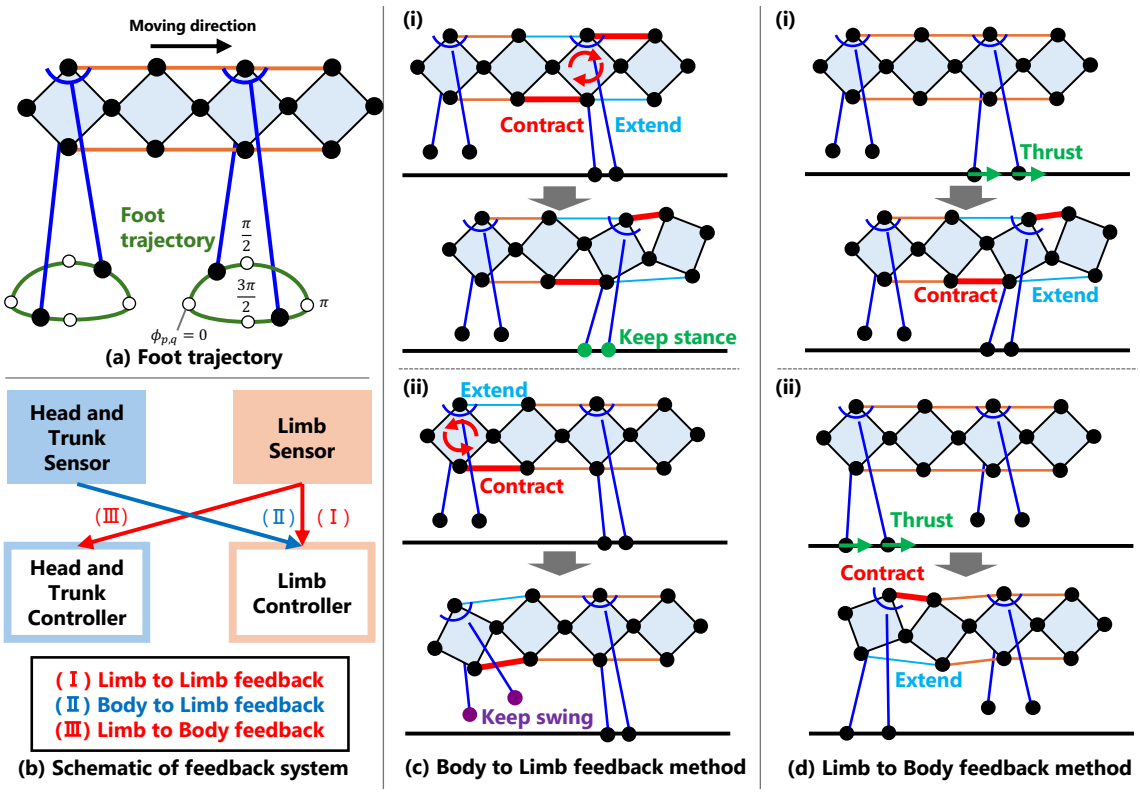


Fig. 2: The proposed control algorithm.

hypothesized that the head and trunk movements play an essential role in determining the flight timing of galloping. To test this hypothesis, we designed a quadruped robot model with a flexible head and trunk as an extension of our previous quadruped model that reproduces walk-trot-gallop gait transitions with trunk movements [13]. The proposed model establishes head-trunk-limb coordination through local sensory feedback mechanisms. The simulation results showed that the strength of the head and trunk actuation serves as a determinant for three types of galloping: gather flight, extended flight, and dual flight.

## 2. MODEL

In our previous work [13], we proposed a decentralized control system based on the interaction between the trunk and limbs. The present model extends this framework by incorporating head dynamics, thereby enabling coordinated control among the head, trunk, and limbs.

### 2.1. Mechanical system

We employed a two-dimensional spring–mass–damper model in the sagittal plane on flat terrain, as shown in Fig. 1. The robot model comprises a head, trunk, and four limbs.

The head and trunk comprise four chained rhombic structures. These rhombic segments are indexed by $i$ from head to hip (i.e. $i$ =1: head, $i$ =2–4: trunk). The mass points connecting the segments are hinge joints that allow ventral flexion and dorsal extension. Furthermore, flexion and extension are actively controlled by linear actuators attached to the ventral and dorsal sides of the body. The actuators are identified by the index $j$ from head to hip ($j$ =1-3) and the index $k$ ($k$ = D for dorsal side, $k$ = V for ventral side).

The limbs are connected to the trunk segments, with two forelimbs attached to segment $i = 2$ and two hindlimbs to segment $i = 4$. Each foot has a mass point equipped with a force sensor detecting the ground reaction force. Both linear and rotary actuators are incorporated into each limb that enable the foot to move along an elliptical trajectory as shown in Fig. 2(a). The limbs are indexed by $p$ ($p$ = R for right, $p$ = L for left) and $q$ ($q$ = F for forelimb, $q$ = H for hindlimb).

### 2.2. Control algorithm

The model implements a decentralized control inspired by the CPG and local sensory feedback. Specifically, as illustrated in Fig. 2(b), three types of feedback control mechanisms are incorporated: (I) and (II) for limbs control, and (III) for control of the head and trunk. The following sections provide detailed descriptions of the control strategies for the limbs and the head and trunk, respectively.

2.2.1. Limb control

We adopted a phase oscillator as the model for CPG. The oscillator phase determines the target length $\bar{l}_{p,q}$ for the linear actuator and the target angle $\bar{\theta}_{p,q}$ for the rotary actuator as follows:

$$\bar{l}^{\mathrm{L}}_{p,q} = \begin{cases} l^{\mathrm{L}}_{\mathrm{n}} - l_{\mathrm{sw}} \sin\phi_{p,q} & (0 \le \phi_{p,q} < \pi) \\ l^{\mathrm{L}}_{\mathrm{n}} - l_{\mathrm{st}} \sin\phi_{p,q} & (\pi \le \phi_{p,q} < 2\pi) \end{cases}, \tag{1}$$

$$\bar{\theta}_{p,q} = -\theta_{\mathrm{a}} \cos\phi_{p,q}, \tag{2}$$

where, $\phi_{p,q}$ denotes the phase of the oscillator assigned to the limb $(p,q)$; $l^{\mathrm{L}}_{\mathrm{n}}$ represents the reference length of the limb; $l_{\mathrm{sw}}$ indicates the amplitude of the target length during the swing phase, while $l_{\mathrm{st}}$ denotes that during the stance phase; $\theta_{\mathrm{a}}$ defines the amplitude of the target angle; $\bar{l}_{p,q}$, $\bar{\theta}_{p,q}$ are tracked using a proportional–derivative (PD) control scheme. As a result, each foot follows an elliptical trajectory, as illustrated in Fig. 2(a).

Next, the time evolution of the phase is described by the following equations:

$$\dot{\phi}_{p,q} = \omega - \sigma_{\mathrm{LL}} N^{\mathrm{V}}_{p,q} \cos\phi_{p,q} + \sigma_{\mathrm{BL}} R_q \cos\phi_{p,q}, \tag{3}$$

$$R_q = \begin{cases} f^{\mathrm{V}}_1 - f^{\mathrm{D}}_1 - f^{\mathrm{V}}_2 + f^{\mathrm{D}}_2 & (q = \mathrm{F}) \\ f^{\mathrm{V}}_3 - f^{\mathrm{D}}_3 & (q = \mathrm{H}) \end{cases}, \tag{4}$$

where $\omega$ is the intrinsic angular velocity of the oscillator; $\sigma_{\mathrm{LL}}$ and $\sigma_{\mathrm{BL}}$ are the weights of the feedback gain; $N^{\mathrm{V}}_{p,q}$ denotes the normal force acting on the limb $(p,q)$; $f^k_j$ represents the force generated in the head and trunk actuator $(j,k)$, defined as positive when acting in the contracting direction. The value of $R_q$ indicate rotation degree of the body segment. For example, $R_{\mathrm{F}}{>}0$ ($f^{\mathrm{D}}_1 + f^{\mathrm{V}}_2 > f^{\mathrm{V}}_1 + f^{\mathrm{D}}_2$) indicates that the segment $i$ =2 experiences a forward rotation force (clockwise force as shown in Fig. 2(c)(i)).

The second term on the right side of Equation (3) constitutes a feedback that relays sensory information from the limb to the limb controller (Fig. 2(b)(Ⅰ)). This corresponds to the local sensory feedback control proposed by Owaki and Ishiguro [8], by which the limb phase is modulated in response to the normal force, generating interlimb coordination.

The third term on the right side of Equation (3) represents feedback from the nearest body actuator (Fig. 2(b)(Ⅱ)). This term adjusts limb phase based on the head and trunk actuation, promoting effective propulsion. For example, as shown in Fig. 2(c)(i), when segment $i = 2$ experiences forward rotation forces ($R_{\mathrm{F}} < 0$), the forelimbs remain in the stance phase. This enables the rotational motion of the trunk to contribute effectively to thrust. In contrast, as shown in Fig. 2(c)(ii), when segment $i = 4$ experiences backward rotation forces ($R_{\mathrm{H}} > 0$), the hindlimbs remain in the swing phase. This enables effective use of trunk rotation to increase stride length. These feedback terms facilitate adaptive head-trunk-limb coordination, supporting efficient propulsion.

Table 1: Simulation parameter of $\beta^k_j$ [m].

| | $\beta^{\mathrm{D}}_1$ | $\beta^{\mathrm{V}}_1$ | $\beta^{\mathrm{D}}_2$ | $\beta^{\mathrm{V}}_2$ | $\beta^{\mathrm{D}}_3$ | $\beta^{\mathrm{V}}_3$ |
|---|---|---|---|---|---|---|
| (a) | 0.196 | 0.140 | 0.140 | 0.140 | 0.112 | 0.112 |
| (b) | 0.112 | 0.112 | 0.021 | 0.021 | 0.042 | 0.042 |
| (c) | 0.196 | 0.168 | 0.168 | 0.168 | 0.168 | 0.140 |

2.2.2. Head and Trunk control

The trunk and head linear actuators is controlled by sensory information from the neighboring limbs (Fig. 2(b)(Ⅲ)). The target length $\bar{l}^k_j$ of the linear actuators is given by the following equations:

$$\bar{l}^{\mathrm{D}}_1 = l^{\mathrm{B}}_{\mathrm{n}} - \beta^{\mathrm{D}}_1 \tilde{N}^{\mathrm{H}}_{\mathrm{F}}, \qquad \bar{l}^{\mathrm{V}}_1 = l^{\mathrm{B}}_{\mathrm{n}} + \beta^{\mathrm{V}}_1 \tilde{N}^{\mathrm{H}}_{\mathrm{F}}, \tag{5}$$

$$\bar{l}^{\mathrm{D}}_2 = l^{\mathrm{B}}_{\mathrm{n}} + \beta^{\mathrm{D}}_2 \tilde{N}^{\mathrm{H}}_{\mathrm{F}}, \qquad \bar{l}^{\mathrm{V}}_2 = l^{\mathrm{B}}_{\mathrm{n}} - \beta^{\mathrm{V}}_2 \tilde{N}^{\mathrm{H}}_{\mathrm{F}}, \tag{6}$$

$$\bar{l}^{\mathrm{D}}_3 = l^{\mathrm{B}}_{\mathrm{n}} - \beta^{\mathrm{D}}_3 \tilde{N}^{\mathrm{H}}_{\mathrm{H}}, \qquad \bar{l}^{\mathrm{V}}_3 = l^{\mathrm{B}}_{\mathrm{n}} + \beta^{\mathrm{V}}_3 \tilde{N}^{\mathrm{H}}_{\mathrm{H}}, \tag{7}$$

$$\tilde{N}^{\mathrm{H}}_q = \sum_p \max\left[0, \tanh(\gamma N^{\mathrm{H}}_{p,q})\right], \tag{8}$$

where $l^{\mathrm{B}}_{\mathrm{n}}$ represents the reference length of the actuator; $\beta^k_j$ and $\gamma$ are the weights of the feedback gain; $N^{\mathrm{H}}_{p,q}$ denotes the thrust force acting on limb $(p,q)$. Each actuator is controlled using a PD controller to achieve its target length.

The second term on the right side of Equation (5)–(7) represents feedback from limb sensory information (Fig. 2(b)(Ⅲ)). For example, as shown Fig. 2(d)(i), when the forelimbs receive thrust from the ground ($\tilde{N}^{\mathrm{H}}_{\mathrm{F}} > 0$), head part bends dorsally ($\bar{l}^{\mathrm{D}}_1 > \bar{l}^{\mathrm{V}}_1$), fore trunk part bends ventrally ($\bar{l}^{\mathrm{V}}_2 > \bar{l}^{\mathrm{D}}_2$). As a result, segment $i = 2$ leans forward, supporting efficient propulsion through coordinated motion of the head and trunk. A similar mechanism applies to the hindlimbs (Fig. 2(d)(ii)), where thrust induces a forward tilt in segment $i = 4$. Together, these feedback mechanisms contribute to support efficient propulsion.

## 3. RESULTS

We conducted simulation experiments to investigate whether multiple gallop patterns could emerge depending on the parameter settings of the proposed model. We hypothesized that changes in the strength of actuation in the head and trunk influence galloping patterns. To test this, we varied the weight of the limb-to-body feedback gain, $\beta^k_j$, as summarized in Table 1. The body mass were chosen based on actual horse's data [14], while the remaining parameters were determined heuristically. The final parameter values were as follows: body length = 1.92 [m], body mass = 500 [kg], $l^{\mathrm{L}}_{\mathrm{n}} = 1.0$ [m], $l_{\mathrm{sw}} = 0.32$ [m], $l_{\mathrm{st}} = 0.0$ [m], $\theta_{\mathrm{a}} = \pi/16.5$ [rad], $\omega = 26$ [rad/s], $\sigma_{\mathrm{LL}} = 0.001$ [rad·kg/m], $\sigma_{\mathrm{BL}} = 0.00001$ [rad·kg/m], $l^{\mathrm{B}}_{\mathrm{n}} = 0.48$ [m], and $\gamma = 0.0005$ [1/N].

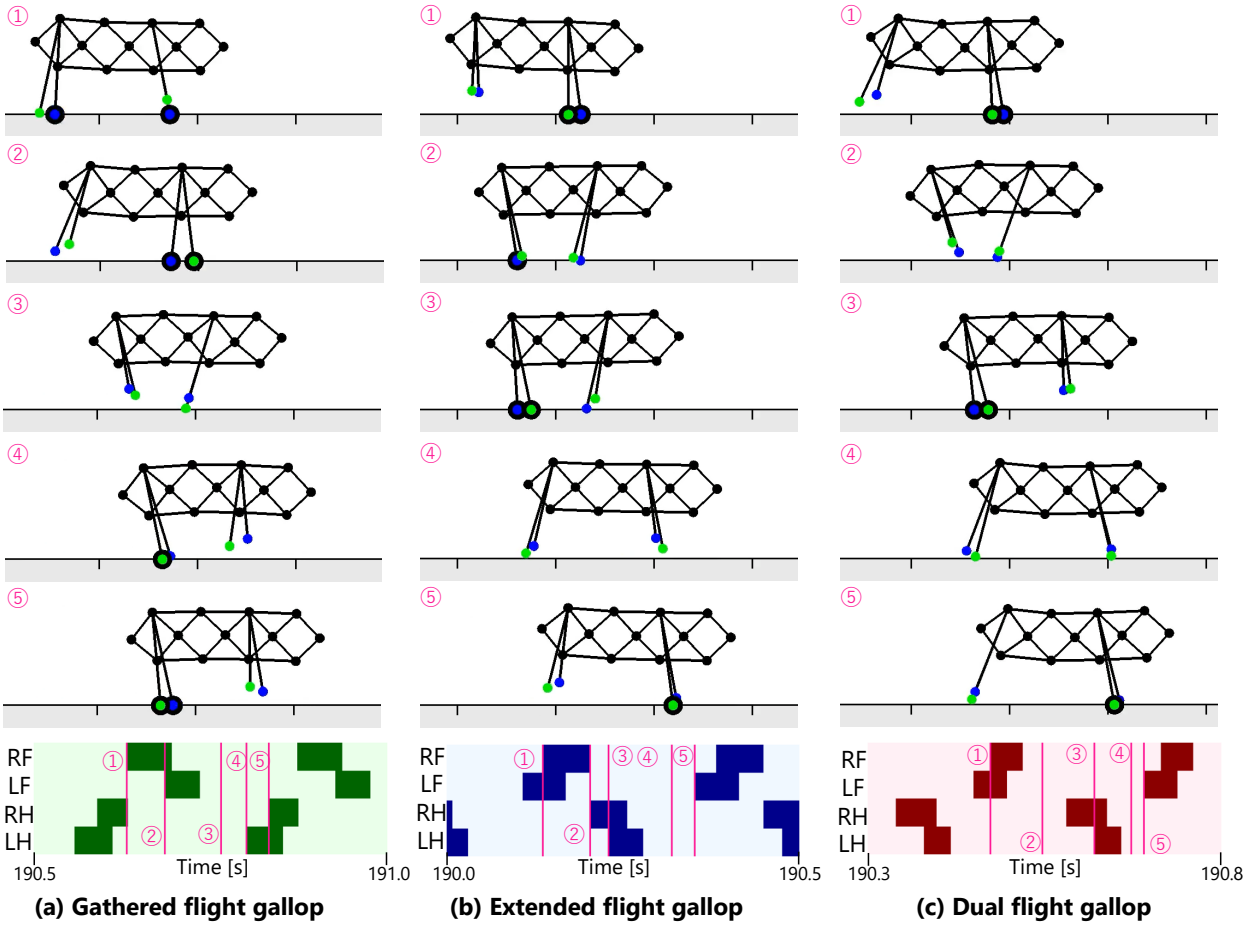


Fig. 3: Results of the simulation. The figure above shows the vertical position of each body part. The figure below is the gait diagram. "RF", "LF", "RH", "LH" mean right forelimb, left forelimb, right hindlimb, left hindlimb. The colored parts indicate that the limbs are on the ground.

By varying three types of $\beta_j^k$ values, we successfully induced three distinct galloping patterns: gathered flight, extended flight, and dual flight gallops. Snapshots and gait diagrams of the simulation results are shown in Fig. 3. In Fig. 3(a), the flight phase follows the forelimb liftoff, characteristic of the gathered flight gallop. In Fig. 3(b), the flight phase occurs after the hindlimb liftoff, indicating an extended flight gallop. In Fig. 3(c), flight phases appear after both forelimb and hindlimb liftoffs, representing a dual flight gallop. As shown in Table 1, the dual flight pattern emerged when the values of $\beta_j^k$ were large, as in case Table 1(c). The extended flight pattern appeared in case Table 1(b), where the trunk feedback gains $(\beta_2^k, \beta_3^k)$ were small relative to the head feedback gain $(\beta_1^k)$. Finally, when neither of these conditions was met, as in case Table 1(a), the gathered flight pattern was observed. These results indicate that varying the feedback gains for the head and trunk segments enables the reproduction of three galloping patterns within a unified control framework.

## 4. CONCLUSION

This study aims to investigate the factors of gallop variation from the aspect of motor control. To this end, we proposed a head–trunk–limb coordination control framework and developed a mathematical model in the sagittal plane. The simulation results demonstrated that the model successfully reproduced three distinct galloping flight patterns in response to the parameters for head and trunk actuation. To the best of our knowledge, this is the first study to reproduce three distinct galloping flight patterns by varying control parameters. This suggests that the proposed control principle may capture a fundamental mechanism that enables locomotion in quadrupedal animals.

Further analysis of the proposed model may provide deeper insights into the roles and importance of head and trunk dynamics during quadrupedal galloping. To this end, future work will explore the relationship between control parameters and flight patterns in this model. Furthermore, we aim to extend the proposed model to three dimensions and conduct experiments with a real robot to validate

and refine the findings in a physical environment.

## ACKNOWLEDGMENT

This work was supported by JSPS KAKENHI Grant Numbers JP22H00203 and JP25K21309.

## REFERENCES

[1] M. Hildebrand, "Motions of the running cheetah and horse", *Journal of Mammalogy*, Vol. 40, No. 5, pp. 481–495, 1959.

[2] Y. Fan, Z. Pei, C. Wang, M. Li, Z. Tang, Q. Liu, "A Review of Quadruped Robots: Structure, Control, and Autonomous Motion", *ADVANCED INTELLIGENT SYSTEMS*, Vol. 6, No. 6, 2024.

[3] M. Hildebrand, "Analysis of asymmetrical gaits", *Journal of Mammalogy*, Vol. 58, No. 2, 1977.

[4] T. Kamimura, S. Aoi, Y. Higurashi, N. Wada, K. Tsuchiya, F. Matsuno, "Dynamical determinants of different spine movements and gait speeds in rotary and transverse gallops." *bioRxiv*, 2020-01.

[5] T. Kamimura, S. Aoi, Y. Higurashi, N. Wada, K. Tsuchiya, F. Matsuno, "Dynamical determinants enabling two different types of flight in cheetah gallop to enhance speed through spine movement", *Scientific Reports*, Vol. 11, No. 9631, 2021.

[6] Y. G. Alqaham, J. Cheng, Z. Gan, "16 Ways to Gallop: Energetics and Body Dynamics of High-Speed Quadrupedal Gaits", *arXiv preprint*, arXiv:2503.13716, 2024.

[7] J. I. Auke and M. A. D. Monica, "Integration of feedforward and feedback control in the neuromechanics of vertebrate locomotion: a review of experimental, simulation and robotic studies", *Journal of Experimental Biology*, Vol. 226, No. 15, 2023.

[8] D. Owaki and A. Ishiguro, "A quadruped robot exhibiting spontaneous gait transitions from walking to trotting to galloping", *Scientific Reports*, Vol. 7, No. 277, 2017.

[9] A. Fukuhara, D. Owaki, T. Kano, R. Kobayashi, A. Ishiguro, "Gait transition to gallop via an interlimb coordination mechanism based on Tegotae from body support and propulsion", *Proceedings of The 8th International Symposium on Adaptive Motion of Animals and Machines*, P26, 2017.

[10] S. Suzuki, D. Owaki, A. Fukuhara, A. Ishiguro, "Quadruped Gait Transition from Walk to Pace to Rotary Gallop by Exploiting Head Movement", *Proceedings of the 5th International Conference on Biomimetic and Biohybrid Systems (Living Machines 2016)*, pp. 532–539, Edinburgh, Scotland, July 2016.

[11] Y. Fukuoka, Y. Habu, T. Fukui, "A simple rule for quadrupedal gait generation determined by leg loading feedback: a modeling study", *Scientific Reports*, Vol. 5, No. 8169, 2015.

[12] T. Fukui, S. Matsukawa, Y. Habu, Y. Fukuoka, "Gait Transition from Pacing by a Quadrupedal Simulated Model and Robot with Phase Modulation by Vestibular Feedback", *Robotics*, Vol. 11, No. 1, 3, 2021.

[13] S. Suzuki, G. Sawada, K. Yasui, A. Fukuhara, A. Ishiguro, "Walk–Trot–Gallop Transition with Spinal Flexion in a Quadruped Model", *Accepted by The 12th International Symposium on Adaptive Motion of Animals and Machines*, 2025.

[14] E. L. Wagner, P. J.Tyler, "A comparison of weight estimation methods in adult horses." *Journal of equine veterinary science*, Vol. 31, No. 12, pp. 706-710, 2011.